Electrochemical growth of iron and cobalt arborescences under a magnetic field

S. Bodea,* R. Ballou,† and P. Molho‡
Laboratoire Louis Néel, CNRS, Boîte Postale 166, 38042 Grenoble Cedex 9, France
(Received 25 August 2003; published 27 February 2004)

Pattern formation in the electrochemical deposition of the magnetic Fe and Co metals from thin layers of $Fe(SO_4)$ or $Co(SO_4)$ aqueous solutions were investigated in circular geometry and under magnetic field. *Sparse* arborescences with few thick branches and *dense* arborescences with many thin branches can be generated when no magnetic field is applied. Unlike for nonmagnetic metals, no tendency towards growth spiraling or asymmetric branching is found out in magnetic field normal to the plane of the growth. The morphology of the deposits appears instead to become more sparse. Under in-plane magnetic field, the sparse arborescences get into a *needle* morphology, oriented along the field, while the dense arborescences show a circular to rectangular morphology symmetry breaking, one edge of the rectangle being parallel to the field. Unexpected in most instances, these magnetic field effects cannot be understood without invoking the magnetic dipolar interaction inside the magnetized growing aggregate together with its interaction with the applied field.

DOI: 10.1103/PhysRevE.69.021605 PACS number(s): 68.70.+w, 81.15.Pq, 05.70.Ln, 75.90.+w

I. INTRODUCTION

Arborescent patterns abound in nature. Almost ubiquitous in botany, they are very often observed in biology or geology as well as in various physical or chemical systems, emerging from growth phenomena [1]. Understanding the mechanisms of these branching morphogenesis and looking for possible universal features in the associated nonequilibrium processes are among the most fascinating but challenging problems [2,3].

A growth phenomenon providing a wealth of insights into pattern formation is the electrochemical deposition (ECD) of metals. Growths in volume from a point, a line, or a plane cathode can be performed [4], but the deposits are very fragile and tend to collapse under their own weight. Quasi-two-dimensional (2D) growths are generally considered, either in circular geometry with an outer ring anode and a central point cathode [5–7] or in parallel geometry with line electrodes [8,9]. A number of patterns can be generated using the same experimental setup [6,7] on changing the growth conditions (e.g., the electric voltage, the electric current, and the concentration of generic or inert species of active impurities or else the thickness of the electrolyte layer). Some of the patterns show the *fractal* features of *diffusion limited aggregation* (DLA) [10] observed in tip-splitting growths. Some others have stable tips and, similar to snowflakes, show *needles* or *dendrites* usually observed in crystal growths [11]. Still others, with unstable tips but a stable envelope growing steadily, dubbed the *dense radial* [12] or *dense branching* morphology (DBM) [13], appear neither fractal nor dendritic. What explains this diversity, not limited to the three instances alluded to, is that several processes are involved in the growths [14].

A magnetic field is an additional external parameter for the ECD of metals that should modify the observed patterns or create new ones. In a wider context, its influence is extremely varied, as found out experimentally, and not fully understood [15,16]. Among the different outcomes, changes in the deposition rates and in the morphology and structure (crystallization or amorphization) of the growths are observed. A variety of other deposit qualities such as adhesion, smoothness, shininess, etc., can as well get modified, opening inviting possibilities of ''tailored'' preparation of materials for applications.

Within the context of morphogenesis phenomena, the effects of magnetic field were first investigated in quasi-2D ECD of Zn, from $Zn(SO_4)$ aqueous solution, in circular geometry [17]. Under increasing magnetic field, applied normal to the plane of the growth, drastic changes of the patterns were observed, either from DLA-like to spiraling DLA, then dense, and finally compact or from dendrites to asymmetric dendrites, then DBM-like, and again compact. Similar growths of Ag, from $Ag(NO_3)$ aqueous solution, evidenced the more intriguing dendritic to spiraling DLA pattern transition, apparently associated with a concomitant change in the rate-determining step from the kinetic to the diffusion processes [18]. Pattern spiraling and/or branching asymmetry appear generic to weak normal field and were also observed in Cu growths, from $Cu(SO_4)$ aqueous solution [19]. An in-plane magnetic field, i.e., applied parallel to the plane of the growth, was applied in the later investigations. Unidirectional stringy patterns, oriented perpendicular to the field, were induced. All these works considered growths of diamagnetic metals (Zn, Ag, Cu) from solutions of diamagnetic (Zn^{2+}, Ag^{+}, NO_3^{-}, SO_4^{2-}) or paramagnetic (Cu^{2+}) ions under static uniform magnetic field. Accordingly, the observed magnetic field effects were essentially discussed in terms of magnetohydrodynamic (MHD) convection induced by the Lorentz force. A magnetic force exists, inherent to concentration gradients and discriminating between diamagnetic and paramagnetic ions, proposed to be of some relevance [20], but is usually ignored.

Additional magnetic forces come into play to influence

*Present address: Institut de Recherche sur les Phénomènes Hors Equilibre, 49 rue Frédéric Joliot Curie, BP 146, F-13384 Marseille cedex 13, France. Email address: simona.Bodea@irphe.univ-mrs.fr
†Email address: ballou@grenoble.cnrs.fr
‡Email address: molho@grenoble.cnrs.fr

the growth processes when the magnetic flux density experienced within the electrochemical cell is no more uniform, either because a magnetic field gradient is externally imposed [21] or because magnetized electrodes are used [22,23], or else because ferromagnetic (or ferrimagnetic) metals are grown under a magnetic field [24,25].

Quasi-2D ECD of a ferromagnetic metal Fe, from $Fe(SO_4)$ aqueous solutions, was previously performed, in parallel geometry and for initial salt concentration fixed at 0.5 mol/l (M), but without magnetic field. Alternating transitions between dendritic and tip-splitting growths were reported [26]. A meshlike pattern was discovered on adding sulfuric acid to the electrolyte solution [27].

The influence of a magnetic field on the pattern formation in quasi-2D ECD of ferromagnetic metals is approached in the present paper, which reports investigations of growths, under fields of different amplitudes and orientations, of Fe and Co, from $Fe(SO_4)$ and $Co(SO_4)$ aqueous solutions, in circular geometry, performed after the discovery of a spectacular morphology symmetry breaking in Fe growths under in-plane magnetic field [24].

II. EXPERIMENTAL DETAILS

An advantage of quasi-2D ECD in circular geometry and local gravity field normal to the electrochemical cell (i.e., with horizontal cell) is that no directional features should be expected in the growth when no magnetic field is applied. A drawback of the circular geometry is that the growth can never be stationary [28], but working at constant voltage and fixed anion concentration in this instance leads to a growth speed profile that is rather flat with respect to the radius of the growing deposit, except near the electrodes of the cell where the speed is larger. Accordingly, at intermediate stages of the growths, it can be approximated during short time as being constant as in stationary growths. A requirement to meet as well is that all the pieces of the electrochemical cell must be nonmagnetic, in order to consider solely the effects of the magnetism of the deposits on their growths and to avoid spurious nonuniformity of the magnetic flux density from one experiment to another, e.g., associated with some undesired magnetic remanence. Using diamagnetic electrodes, different from the grown metals, can of course lead to changes in the electrolyte composition through anodic dissolution, but the corresponding influence on the growths should take place only when the deposits are already large, of about half of the anode diameter.

The experiments were performed at constant voltage, applied between a Cu ring anode, of diameter 4 cm and thickness 0.5 mm, and a central Cu ''point'' cathode, in fact the end of a Cu wire, of diameter 0.05 mm. A thin film ($\approx$500 μm thick) of an electrolyte solution is spread on a glass plate, edged by the anode. A clean microscope coverslip, of thickness 0.14 mm, is put under the cathode in order to reduce locally the thickness of the liquid film and to allow one to remove the deposit out of the solution after the growth. Unlike in earlier similar experiments [6,7], no glass plate is positioned above the solutions: the upper surface of the electrolyte film is left free to reduce the destroying effect on the deposits of the H_2 bubbles generated during the growth. All the growths were made without supporting electrolyte and from aqueous solutions prepared by dissolving in deionized water the appropriate amounts of commercial ferrous $[Fe(SO_4)\cdot 7H_2O]$ or cobalt $[Co(SO_4)\cdot xH_2O]$ sulfate salts [29]. A solution is freshly prepared for each new growth to avoid aging effects. The entire setup can be temperature regulated and is placed in a transparent Plexiglas box isolating the growth from external perturbations (Fig. 1). Each growth is done at 20 °C and takes few minutes.

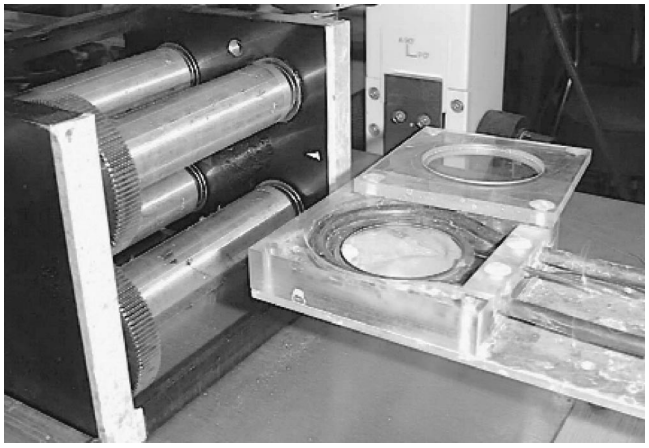

FIG. 1. Experimental setup. On the right the electrochemical cell within its Plexiglas box. On the left the magnetic mangles generating the uniform magnetic field.

Two different devices are used to generate the magnetic field: a ''magnetic mangle'' and an electromagnet. The magnetic mangle consists of four cylindrical magnets (Fig. 1), each one magnetized perpendicular to its axis, disposed in such a way that a uniform magnetic field is obtained in a volume of about $2\times2\times2$ cm^3 [30]. By appropriately rotating the magnets, the amplitude of the magnetic field can be varied from -0.2 to 0.2 T [31]. The electromagnet has a distance of 4 cm between the pole pieces and can generate magnetic fields up to 1.6 T. The electrochemical cell used in this case is smaller, with an anode of diameter 2.8 cm. The electromagnet allows higher and more uniform fields, while the magnetic mangle, a compact system easy to handle, allows *in situ* microscopic observations. Both devices show the same effects of the magnetic field on the growth, in the common range of amplitude. Changing the field direction with respect to the plane of growth on the electromagnet can only be made by orienting the electrochemical cell from horizontal to vertical, which will not be possible for open cells. This drawback does not exist with the magnetic mangle which can easily be rotated as a whole to change the magnetic field direction.

An optical microscope, a charge-coupled device camera, a video recorder, and an image processing system are used to perform *in situ* observations during the growth and at different scales. Postdeposited analyses are more delicate than *in situ* ones: the deposits, floating in the aqueous solution, are very fragile so that removing them out of the solution can lead to a destruction of the very small branches as well as an oxidization.

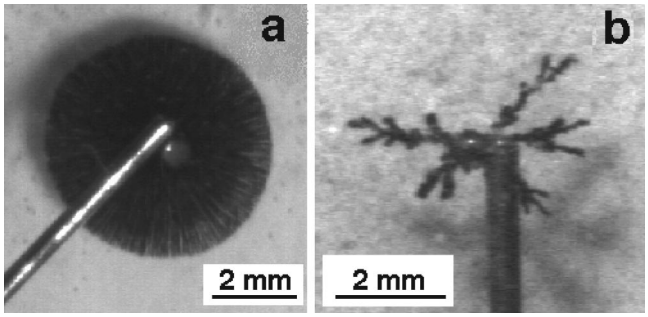

FIG. 2. Iron electrodeposits generated without magnetic field (a) for $\mathcal{C}=6\times10^{-2}$ M and $\mathcal{U}=5$ V (*dense* morphology), (b) for $\mathcal{C}=5\times10^{-1}$ M and $\mathcal{U}=5$ V (*sparse* morphology). The metallic rod in both images is above the plane of the growth and is a guiding tube for the cathode.

III. GROWTHS WITHOUT MAGNETIC FIELD

Growths at different initial concentrations $\mathcal{C}$ of salts, either $Fe(SO_4)$ or $Co(SO_4)$, and at different values of the constant electric voltage $\mathcal{U}$ applied between the electrodes were attempted. A major limiting factor was the hydrogen evolution reaction leading to the formation of H_2 bubbles that alters the deposit, by isolating branches from the electrolyte, and even destroys it. This was fortunately not the case for all the values of $\mathcal{C}$ and $\mathcal{U}$.

No chemical additive was considered, at least in the first step of the investigations and to limit the number of control parameters that can be modified. The initial pH of the solution was thus measured but not changed by addition of an acid or a base to have it constant with respect to $\mathcal{C}$. A growth parameter that was not fixed with accuracy, because no upper glass plate is positioned above the solutions, is the electrolyte thickness. Nevertheless its value, from one growth to another, is controlled by always spreading the same volume of electrolyte on the lower glass plate of the electrochemical cell.

A. Iron arborescences

Growths of Fe arborescences unaltered by the formation of H_2 bubbles could be performed for $\mathcal{C}$ between 3×10^{-2} M and 5×10^{-1} M and $\mathcal{U}$ between 3 V and 7 V. The measured initial pH of the solutions was $p\mathrm{H}=3.60(5)$ for $\mathcal{C}=6\times10^{-2}$ M, $p\mathrm{H}=3.40(5)$ for $\mathcal{C}=10^{-1}$ M, and $p\mathrm{H}=2.95(5)$ for $\mathcal{C}=5\times10^{-1}$ M, varying roughly as $-\frac{1}{2}\log_{10}(\mathcal{C})$ for intermediate $\mathcal{C}$, as expected.

Within the $\mathcal{C}$ range from 3×10^{-2} M to 10^{-1} M the macroscopic morphology of the deposits is always dense and isotropic, similar to those reported earlier as DBM [12,13]: a stable circular envelope increasing uniformly in size is observed, with branches which, although hard to distinguish at this scale, appear to grow radially, outward from the central cathode [Fig. 2(a)].

When $\mathcal{C}$ is between 10^{-1} M and 5×10^{-1} M, the macroscopic morphology of the deposits, still dense at the beginning of the growth, soon become sparse with fewer and thicker branches [Fig. 2(b)]. The larger $\mathcal{C}$ is the sooner is the change, being practically immediate for $\mathcal{C}=5\times10^{-1}$ M.

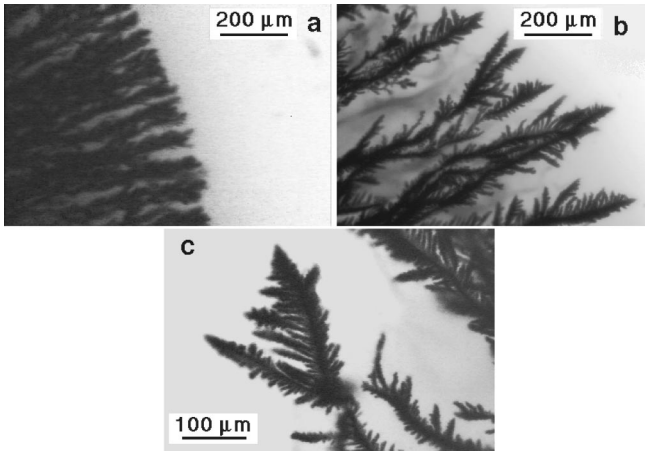

FIG. 3. Microscope view of the iron electrodeposits generated without magnetic field for $\mathcal{C}=6\times10^{-2}$ M and $\mathcal{U}=5$ V (dense morphology) (a) at the beginning of the growth, (b) and (c) at the end of the growth.

Observations at different scales using the microscope showed that the morphology of the deposits evolves during the growth, even in the case of the dense arborescences: the growth starts with a dense, radial, and isotropic deposit, unfortunately so dense that the fine structure of the branches is hard to resolve experimentally [Fig. 3(a)]. As the growth proceeds, the deposit becomes less dense and more dendritic [Fig. 3(b)], owing to the gradual change during the growth of the salt concentration profile and of the electric current, leading in turn to an evolving growth speed of the branches [28,32]. A well defined angle exists between the main and the side branches of the dendrites [Fig. 3(c)]. Nevertheless the orientation of the branches is only local and not preserved over large distances, contrary to that in usual dendritic growths [6,7]. An outcome of the underlying distribution of orientations over the different possible directions is that the pattern at the macroscopic scale appears radial isotropic with a stable circular envelope.

Examinations of the smallest branches of the arborescences could be performed by transmission electron microscopy (TEM) combined with selected area electron diffraction (ED). Detailed elsewhere [33], these investigations allowed us to extend the observations of the morphology down to the nanometric scale and to determine the atomic structure of the deposits. Single crystalline dendrites of pure Fe with the body centered cubic (bcc) structure were systematically observed in all the instances, independent of the growth conditions (Fig. 4). Nucleations of ordered microdomains of the face centered cubic (fcc) phase of Fe into the main bcc phase were also detected but at very weak density, as well as impurities of Fe oxide (Fe_3O_4) and anhydrous Fe sulfate ($FeSO_4$) but at practically evanescent quantities and most probably on the surface. The first main conclusion of these investigations is that, although showing similar macroscopic morphology features, the dense arborescences can rigorously not be fully assimilated to those mentioned as having the DBM morphology in the literature. Generally these are associated with tip-splitting processes at the microscopic scale, which should lead to a noncrystalline deposit. The second

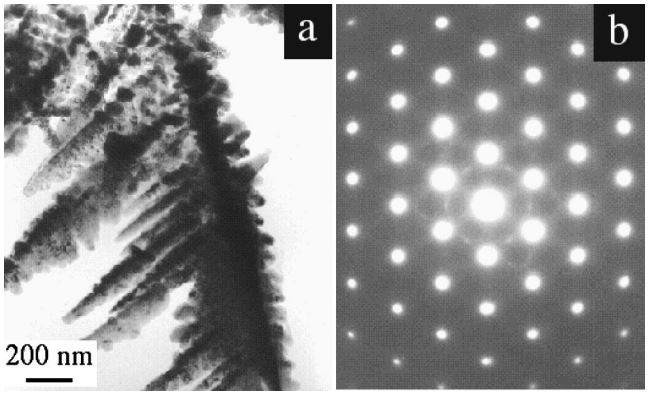

FIG. 4. (a) TEM image and (b) ED pattern of a portion of an iron electrodeposit generated without magnetic field for $\mathcal{C}=6\times10^{-2}$ M and $\mathcal{U}=5$ V. Similar TEM images and ED patterns are obtained for other growth conditions: dense arborescences cannot be distinguished from sparse arborescences at the scales of the TEM observations.

main conclusion is that at scales up to about 1 μm, the deposits are always single crystalline, more precisely dendrites with a branching angle of 60°, which can be interpreted in terms of branches growing along the twofold axes perpendicular to the same threefold axis among the four of the bcc structure. The loss of the branch orientation and subsequently of the crystalline coherence should occur at larger scales.

B. Cobalt arborescences

Growths of Co arborescences unaltered by the formation of H_2 bubbles could be performed for a $\mathcal{C}$ range only between 10^{-1} M and 5×10^{-1} M, i.e., even smaller than that for the Fe arborescences, and for $\mathcal{U}$ between 3 V and 8 V. The initial pH of the solutions could not be measured, but is estimated to $p\mathrm{H}\approx4.3$ for $\mathcal{C}=10^{-1}$ M and $p\mathrm{H}\approx3.9$ for $\mathcal{C}=5\times10^{-1}$ M, from that given in the Merck chemical databases [34] and assuming that it varies with $\mathcal{C}$ as $-\frac{1}{2}\log_{10}(\mathcal{C})$.

A single macroscopic morphology of the deposits is always generated, very similar to that obtained with Fe in the same, 10^{-1} M–5×10^{-1} M, $\mathcal{C}$ range, i.e., dense at the beginning of the growth but soon becoming sparse with fewer and thicker branches [Fig. 5(a)] as the growth proceeds. Again the larger $\mathcal{C}$ is, the sooner is the change.

Growths at limited currents were tried. These are made at constant voltage $\mathcal{U}$ as far as the current remains lower than a limiting value $\mathcal{I}$, but at constant current equal to $\mathcal{I}$ otherwise. Dense deposits, similar to that observed with Fe at constant voltage, could be obtained in this way but in the $\mathcal{C}$ range from 3×10^{-2} M to 10^{-1} M and for $\mathcal{I}$ lower than a critical value $\mathcal{I}_0$ (~3 mA for $\mathcal{U}=5$ V) [Fig. 5(b)]. A sparse morphology emerges invariably when $\mathcal{I}\geqslant\mathcal{I}_0$.

Observations at different scales using the microscope were performed as with the Fe arborescences and led to similar conclusions. A slight difference however exists, concerned with the dense arborescences, which with Co appeared still more dense, with a fine structure that often cannot be distinguished by optical microscopy, even at the

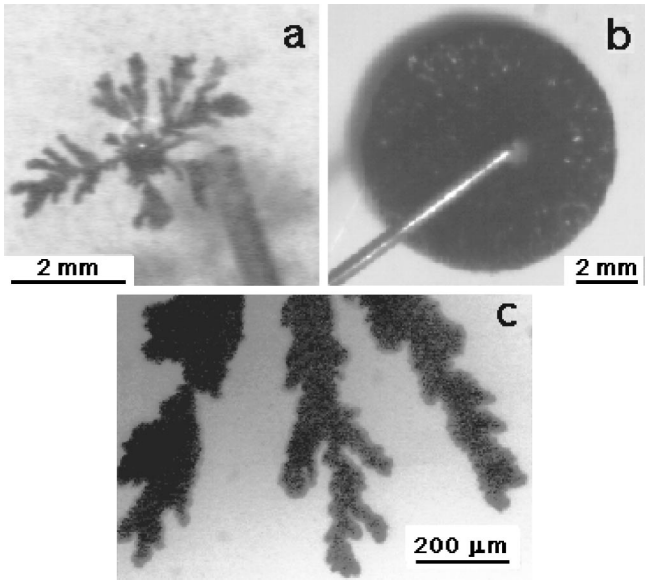

FIG. 5. Cobalt electrodeposits generated without magnetic field (a) at constant voltage for $\mathcal{C}=5\times10^{-1}$ M and $\mathcal{U}=5$ V (sparse morphology), (b) at limited current for $\mathcal{C}=5\times10^{-1}$ M, $\mathcal{U}=5$ V, and $\mathcal{I}\leqslant\mathcal{I}_0\sim3$ mA (dense morphology). (c) Microscope view of the cobalt electrodeposits generated at constant voltage (sparse morphology).

end of the growths. A spatial resolution is also lacking for both the Fe and Co sparse arborescences, the branches of which appear coarse [Fig. 5(c)] but could as well consist in much thinner branches grouped as in a cypress tree. A preliminary x-ray μ-imaging experiment, using synchrotron radiation and combining absorption and phase contrast, confirmed that this is most probably the case: the x-ray image clearly reveals a fibrous texture not visible by optical microscopy (Fig. 6).

Co arborescences could also be examined by TEM combined with selected area ED [33]. Single crystalline dendrites of pure Co with the hexagonal compact (hcp) structure were systematically observed. Again, impurities of Co oxide (Co_3O_4) and anhydrous Co sulfate ($CoSO_4$) were detected but at very small amounts, most probably on the surface. A growth of the branches along the twofold axes perpendicular to the sixfold axis of the hcp structure was evidenced.

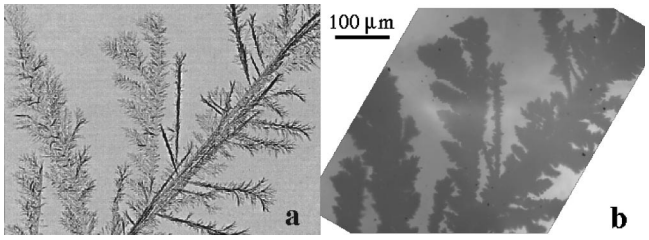

FIG. 6. (a) X-ray image of a portion of a cobalt electrodeposit generated without magnetic field at constant voltage for $\mathcal{C}=5\times10^{-1}$ M and $\mathcal{U}=5$ V (sparse morphology), as obtained by synchrotron radiation μ imaging with combined absorption and phase contrast. (b) Optical image of the same portion of the electrodeposit.

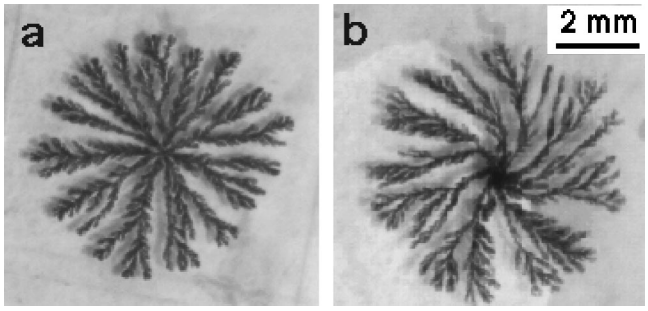

FIG. 7. Zinc electrodeposits generated for $\mathcal{C}=10^{-2}$ M and $\mathcal{U}=5$ V (a) without magnetic field, (b) under a normal magnetic field $\vec{H}_{\perp}$ of 0.2 T pointing towards the observer.

IV. GROWTHS UNDER NORMAL MAGNETIC FIELD

Growths under magnetic field $\vec{H}_{\perp}$ applied normal to the plane of the growth were performed at the different conditions which without magnetic field led to the dense and sparse arborescences for both Fe and Co. Growths of Zn arborescences from $Zn(SO_4)$ aqueous solutions were additionally made on the same experimental setup for comparison. With open electrochemical cells, the electromagnet could not be used since a horizontal magnetic field was produced. Accordingly, except for a few experiments with closed cells positioned vertically, all the growths were made for $\vec{H}_{\perp}$ between -0.2 T and 0.2 T, using the magnetic mangle.

An example of a Zn deposit grown under $\vec{H}_{\perp}$ is shown in Fig. 7 and compared to that obtained under the same conditions but without magnetic field. A tendency of the morphology to spiral is found out, with branches gyrating counterclockwise, when going over them from the point they started growing to the point they stopped growing, for $\vec{H}_{\perp}$ pointing towards the observer. Although not systematically, the main branches show some asymmetry as well, i.e., have more elongated secondary branches on one side of the central nerve than on the other. On inverting $\vec{H}_{\perp}$ the branches gyrate clockwise and the weak asymmetry of the main branches appear to change to the opposite. A small amount of engine oil can be added to the electrolyte and, by simple shaking, emulsified within it, without inducing any apparent change of the morphology, while leading to the formation in the solution of optically opaque microdroplets, the trajectories of which, visualizing the fluid motion, can be followed. A global motion was detected which, for $\vec{H}_{\perp}$ pointing towards the observer, corresponded to a counterclockwise fluid rotation. This confirmed the occurrence of the expected MHD convection induced by the Lorentz force once $\vec{H}_{\perp}$ is applied.

The effect of $\vec{H}_{\perp}$ on the morphology of the deposits obtained in both the Fe and Co growths differs completely from that in the Zn growths. Neither clear-cut spiral feature nor branch asymmetry appears to emerge. Subtle changes seem nevertheless to be induced.

Whatever the amplitude of $\vec{H}_{\perp}$, within the experimental available range, and for initial salt concentration $\mathcal{C}$ between 3×10^{-2} M and 10^{-1} M, the macroscopic morphology of the deposits obtained in the Fe growths remain always dense, isotropic, with a stable circular envelope increasing uniformly in size, but the branches appear to become less ramified when the amplitude of $\vec{H}_{\perp}$ is increased (Fig. 8). *In situ* observations at different scales performed during the growth showed features similar to those observed in growths without magnetic field. Some slight differences were however found out, which are best revealed in the less dense portions of the deposits, at the end of the growths: on increasing $\vec{H}_{\perp}$ the local morphology of the arborescences gets more sparse, with less branches more separated from each other. Small branches were from time to time pulled out of the deposit and rejected close to the anode, owing to an underlying strong stirring of the electrolyte, but apparently not as frequently as to be the sole cause of the increased sparseness of the deposits. As for Zn the presence of MHD convection was again evidenced using emulsified oil.

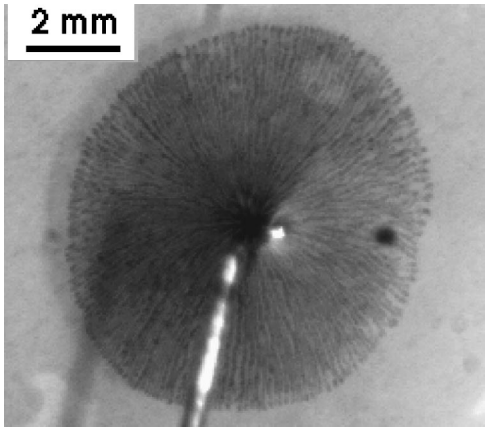

FIG. 8. Iron electrodeposit generated for $\mathcal{C}=6\times10^{-2}$ M and $\mathcal{U}=5$ V under a normal magnetic field $\vec{H}_{\perp}$ of 0.2 T pointing towards the observer.

When the initial salt concentration $\mathcal{C}$ is between 10^{-1} M and 5×10^{-1} M, sparse arborescences are generally obtained in both the Fe and Co growths, for all the available amplitudes of $\vec{H}_{\perp}$. Slight changes in the macroscopic morphology are again found out, with, in particular, branches that appear to become more ramified on increasing the amplitude of $\vec{H}_{\perp}$ (Fig. 9). The mechanical effects on the growing deposits of the fluid motions under $\vec{H}_{\perp}$ are more destroying, since now even macroscopic branches are from time to time pulled out of the deposit and rejected close to the anode. Very few branches remain in some growths, in which case they show a gyration tendency recalling a spiral pattern. Another more microscopic feature of the growths under $\vec{H}_{\perp}$, revealed by the *in situ* observations at different scales, is that the small branches tend often to either collapse over each other, to form progressively thicker branches, or move aside from each other, so as to be distinguished at larger scales, leading thus to an apparently more ramified macroscopic morphology. Once more the presence of MHD convection could be proven using emulsified oil.

Arborescences grown under $\vec{H}_{\perp}$ were also examined by TEM combined with selected area ED [33]. Single crystal-

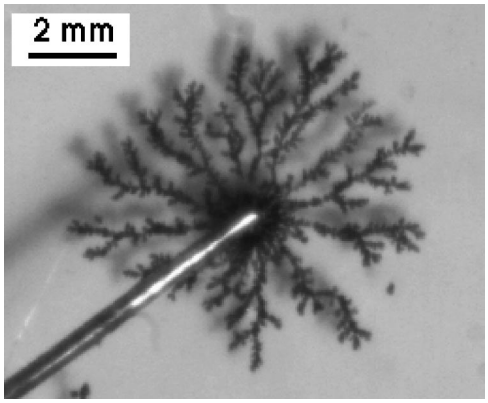

FIG. 9. Cobalt electrodeposit generated for $\mathcal{C}=5\times10^{-1}$ M and $\mathcal{U}=5$ V under a normal magnetic field $\vec{H}_{\perp}$ of 0.2 T pointing towards the observer.

line dendrites with the same structures, bcc for Fe and hcp for Co, as those of deposits grown without magnetic field are observed, but with $\vec{H}_{\perp}$-induced specific features that depend on whether Fe or Co arborescences are under concern. Curiously, the Fe dendrites were bent, reminding the spiral observed at the macroscopic scales in the Zn growths. Concomitantly the ED pattern show arched spots that are well interpreted in terms of a gradual rotation of the twofold axis along which the dendrite grows or, equivalently, a progressive torsion of the crystal, around a threefold zone axis parallel to $\vec{H}_{\perp}$. This further confirmed the tendency towards a spiral morphology, which thus appears to exist at scales up to at least 1 μm but to be inhibited for some reason at large scales. Completely different, the effect of $\vec{H}_{\perp}$ on the Co dendrites is to tip up the sixfold axis of the hcp structure from the direction normal to the plane of the growth to an in-plane direction, leading to dendrites growing now along the sixfold axis and with a branching angle of 90°. The origin of this $\vec{H}_{\perp}$-induced change of the growth axes is so far unclear.

V. GROWTHS UNDER IN-PLANE MAGNETIC FIELD

Growths of both Fe and Co under magnetic field $\vec{H}_{||}$ applied parallel to the plane of the growth were also performed, systematically for the different values of $\mathcal{C}$ and $\mathcal{U}$. The electromagnet could be used in this instance. It mostly allowed us to check whether the morphology changes of the Fe and Co deposits induced under $\vec{H}_{||}$ are reproduced with more uniform magnetic fields and are not ascribable to the residual magnetic field gradients existing in the magnetic mangle [30].

Owing to the geometry itself of the quasi-2D ECD growths, it should qualitatively be expected that the average velocity of the moving charges in the solution will essentially be parallel to the plane of the growth, i.e., will have a negligible component perpendicular to $\vec{H}_{||}$, implying that no MHD convection induced by the Lorentz force should occur. According to Ref. [35] however, a gravitoconvection may occur even within thin horizontal electrolyte layers that leads to the formation of spatial structures in the fluid flows with

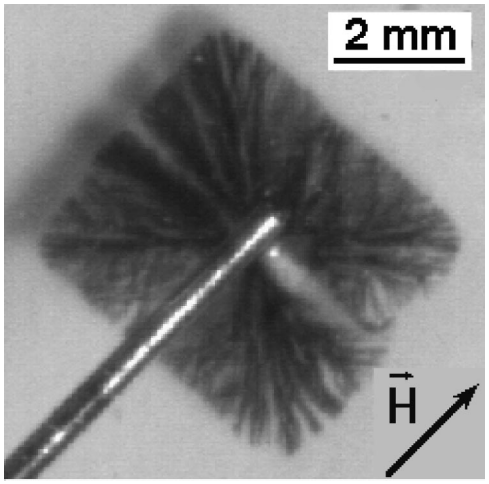

FIG. 10. Iron electrodeposit generated for $\mathcal{C}=6\times10^{-2}$ M and $\mathcal{U}=5$ V under an in-plane magnetic field $\vec{H}_{||}$ of 0.2 T. The arrow indicates the orientation of the applied magnetic field within the plane of the growth.

ascending or descending motions of the ions, near the electrodes, and similar small regions in the bulk of the electrolyte. This could induce local MHD convection.

Growths of Zn from $Zn(SO_4)$ aqueous solutions on the same experimental setup were again considered for comparison. No specific change of the morphology was found out between the growths without magnetic field and the same growths under $\vec{H}_{||}$ using the magnetic mangle. No MHD convection could clearly be identified under $\vec{H}_{||}$ up to 0.2 T.

A. Iron arborescences

A spectacular morphology symmetry breaking is induced in the growths of Fe under $\vec{H}_{||}$, for $\mathcal{C}$ within the range from 3×10^{-2} M to 10^{-1} M that leads to the dense arborescences when no magnetic field is applied. As already reported [24], for growths with $\mathcal{C}=6\times10^{-2}$ M the macroscopic morphology of the deposits is still dense, but less than in the growths without magnetic field and, above all, no more isotropic: the circular envelope increasing uniformly in size under zero field is transformed into a rectangular envelope centered on the initial point cathode with clean edges, two of which are always along $\vec{H}_{||}$ and the two others are along the direction perpendicular to $\vec{H}_{||}$ within the plane of growth (Fig. 10). While without magnetic field the branches appear to grow radially outward from the central cathode, under $\vec{H}_{||}$ they grow according to a more complex texture, apparently straight along the diagonals of the rectangle and building a straight front in the directions parallel and perpendicular to the field. An absence of growth from the initial point cathode in the direction perpendicular to $\vec{H}_{||}$ is often observed. Around an $\vec{H}_{||}$ amplitude of 0.2 T, the rectangular shape is stabilized from almost the beginning of the growths and increases homothetically in size, as the growth proceeds, with straight fronts propagation. It does not depend on initial conditions as demonstrated by starting the growth without mag-

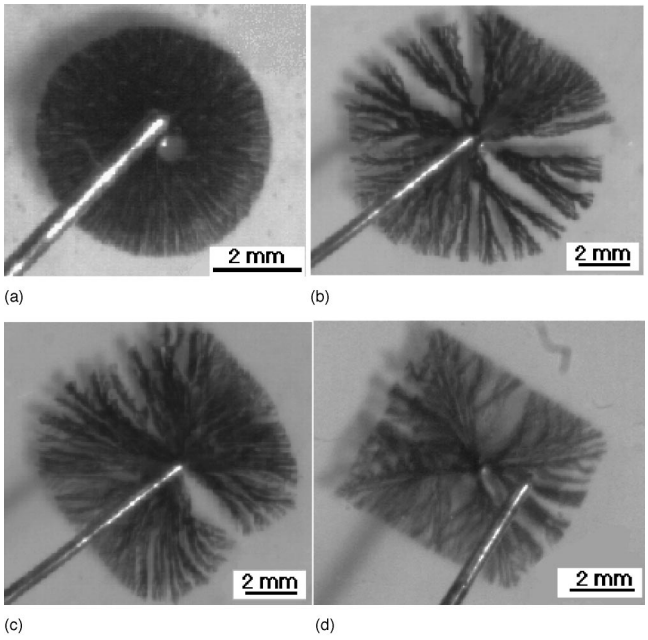

FIG. 11. Iron electrodeposit generated for $\mathcal{C}=6\times10^{-2}$ M and $\mathcal{U}=5$ V under an in-plane magnetic field $\vec{H}_{||}$ of (a) 0 T, (b) 0.04 T, (c) 0.14 T, and (d) 0.2 T. $\vec{H}_{||}$ is always along the guiding tube for the cathode.

netic field and applying $\vec{H}_{||}$ a little later: the circle to rectangle transition takes place during the growth, once $\vec{H}_{||}$ is switched on.

On performing the growths at different amplitudes of $\vec{H}_{||}$, it is found out that the change of the macroscopic morphology of the deposits, from dense and circular in zero field [Fig. 11(a)] to less dense and fully rectangular in large field [Fig. 11(d)], is gradual. An increased sparseness is observed in already rather low field amplitude with a texture of branch less radial and showing a tendency to form straight growth fronts [Fig. 11(b)]. An absence of growth from the initial point cathode in the direction perpendicular to $\vec{H}_{||}$ is already manifested. On further increasing the field amplitude, no further sparseness is qualitatively induced while the rectangular shape is progressively stabilized with more clean edges but still rounded corners [Fig. 11(c)]. A fully perfect rectangle is practically achieved around the maximum amplitude of $\vec{H}_{||}$ provided by the magnetic mangle. Growths were performed under larger $\vec{H}_{||}$, up to 1.6 T using the electromagnet. No basic change was found out: a deposit with practically the same rectangular shape and the same branch texture is generated. The aspect ratio of the rectangle is not field dependent but can show slight changes from one growth to the other.

Observations at different scales using the microscope showed that the main effect of $\vec{H}_{||}$ is to induce a growth of the branches at a definite angle from a fixed direction, either $\pm\phi\approx30°$ from the $\vec{H}_{||}$ direction [Fig. 12(a)] or $\pm\psi\approx30°$ from the perpendicular to it in the plane of the growth [Fig. 12(b)]. Assuming then that these branches grow at the same speed, two pairs of parallel straight growth fronts perpendicular to each of the fixed directions are generated by mere geometry. An isosceles triangle pattern is associated with each straight growth front, with the initial point cathode as its summit, the angle $2\times\phi$ or $2\times\psi$ as its angle at the summit, and the growing front as its base. Associated with the two perpendicular fixed directions under concern, we get four triangles inscribed in a square envelope if $\phi=\psi$ and the growth speed of the branches is the same along any direction. A rectangular envelope is instead observed, indicating that the previous constraints are not met. A difference in morphology between those in Figs. 12(a) and 12(b) is in fact apparent. Also the angle $\pm\phi$ is less sharply defined than the angle $\pm\psi$. Geometrically there are voids between the triangles. These are experimentally filled with more stringy branches and are the regions where the ϕ or ψ angles differ the most from 30°. The observed absence of growth from the initial point cathode in the direction perpendicular to $\vec{H}_{||}$ is unexplained, but is a further indication that the growth along and perpendicular to $\vec{H}_{||}$ should differ somehow.

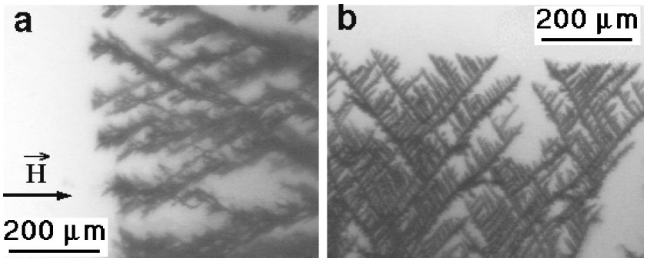

FIG. 12. Microscope view of the growing iron electrodeposit generated for $\mathcal{C}=6\times10^{-2}$ M and $\mathcal{U}=5$ V under an in-plane magnetic field $\vec{H}_{||}$ of 0.2 T (a) at a front perpendicular to it, (b) at a front parallel to it.

A tendency to form a straight growth front under $\vec{H}_{||}$ still exists for $\mathcal{C}$ a little larger than 10^{-1} M, more precisely for $\mathcal{C}$ in the rather fuzzy range within which without magnetic field the morphology transition from the dense to the sparse arborescences takes place. Under $\vec{H}_{||}$, the deposits at the end of the growths are usually clearly sparse at the macroscopical level, but often show dense regions where the straight growth fronts are observed (Fig. 13). Actually, as without magnetic field, the growths evolve in time, starting as dense

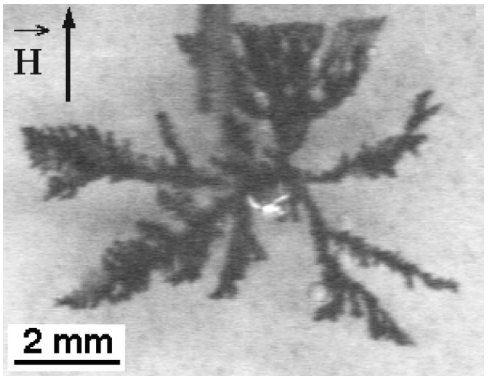

FIG. 13. Iron electrodeposit generated for $\mathcal{C}=2\times10^{-1}$ M and $\mathcal{U}=5$ V under an in-plane magnetic field $\vec{H}_{||}$ of 0.2 T.

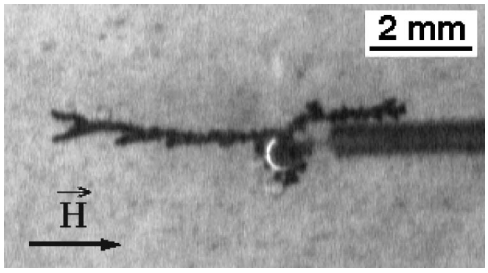

FIG. 14. Iron electrodeposit generated for $\mathcal{C}=5\times10^{-1}$ M and $\mathcal{U}=5$ V under an in-plane magnetic field $\vec{H}_{||}$ of 0.2 T.

before becoming sparse. Apparently, under $\vec{H}_{||}$ the dense regime would either be better stabilized during the growth for some reason or be better put into evidence owing to the straight growth fronts associated with it. A slight difference with the growths without magnetic field is found out: the branches of the deposits grown under $\vec{H}_{||}$ appear always more dendritic at the macroscopic level.

On increasing $\mathcal{C}$ the tendency to form a straight growth front dwindles out while the deposits become more and more sparse. When $\mathcal{C}$ is close to 5×10^{-1} M, the macroscopic morphology of the deposit grown under $\vec{H}_{||}$ is completely different. It is now stringy and shows systematically two main branches growing, in opposite directions from the cathode, along $\vec{H}_{||}$ (Fig. 14). Any growth of branches along other directions appear to be blocked up. A stringy deposit as any magnetic needle shape material will always align itself along an applied magnetic field to minimize the magnetostatic Zeeman interaction. So its orientation along the $\vec{H}_{||}$ direction was somehow expected. At the $\mathcal{C}$ under concern, sparse arborescences are also obtained when no magnetic field is applied, but not limited to two branches. Accordingly either some additional mechanism is at work to inhibit the growth of branches in directions different from $\vec{H}_{||}$ or these branches mechanically twist along $\vec{H}_{||}$ while growing to bind with each other and form a single thick branch. A similarity in the change of the patterns on applying $\vec{H}_{||}$ with those formed under magnetic field by aggregation of magnetic microspheres interacting via magnetic dipolar interactions [36] should be emphasized.

Arborescences of Fe grown under $\vec{H}_{||}$ were examined by TEM combined with selected area ED [33]. Curiously, no specific features were observed that would reveal that $\vec{H}_{||}$ was applied during the growth, whatever the possible values of $\mathcal{C}$, except for a slight tendency to the formation of more needlelike branches on increasing the amplitude of $\vec{H}_{||}$. Accordingly the mechanism of the drastic $\vec{H}_{||}$-induced morphology changes, observed macroscopically and with the optical microscope, should operate at scales larger than that (~1 μm) accessed by TEM.

B. Cobalt arborescences

No dense arborescences of Co could be generated at constant voltage, without being strongly altered by the hydrogen evolution reaction and the subsequent formation of H_2 bubbles. Accordingly, unlike with the Fe arborescences under $\vec{H}_{||}$, no circle to rectangle morphology symmetry breaking could effectively be observed. Attempts were made to induce the expected morphology transition in growths at limiting current but were not successful, owing most probably to the strong time dependent features of such growths and transitory effects. Growths of Co under $\vec{H}_{||}$ for $\mathcal{C}$ close to 2×10^{-1} M lead however to deposits, the morphology of which bear strong analogy with that of Fe in the same conditions (Fig. 15). Although perhaps not as clear as in the Fe growths, a tendency to form straight growth fronts under $\vec{H}_{||}$ is manifested. This would indicate that the circle to rectangle morphology transition could be observed in Co growths if not thwarted by hydrogen evolution.

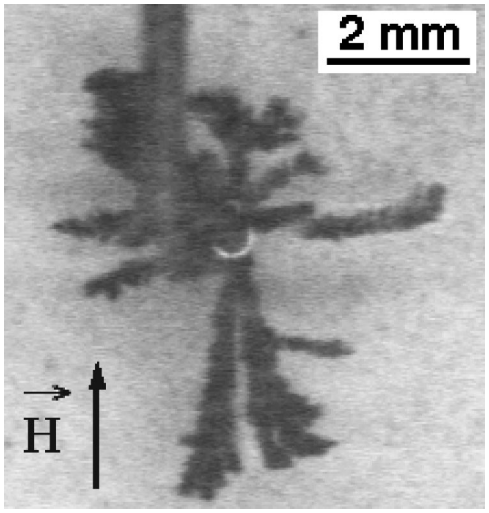

FIG. 15. Cobalt electrodeposit obtained for $\mathcal{C}=2\times10^{-1}$ M and $\mathcal{U}=5$ V under an in-plane magnetic field $\vec{H}_{||}$ of 0.2 T.

Another additional similarity, between Fe and Co, in the morphology response to an applied magnetic field is that observed in the growths under $\vec{H}_{||}$ for $\mathcal{C}$ close to 5×10^{-1} M. A stringy macroscopic morphology is induced in the Co growths as well, with again systematically two main branches growing, in opposite directions from the cathode, along $\vec{H}_{||}$ (Fig. 16). All the other branches are much smaller and show a tendency to align themselves along $\vec{H}_{||}$ during

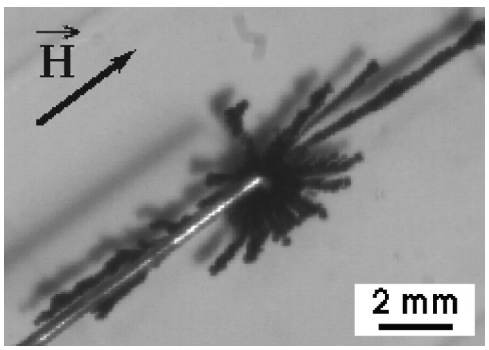

FIG. 16. Cobalt electrodeposit obtained for $\mathcal{C}=5\times10^{-1}$ M and $\mathcal{U}=5$ V under an in-plane magnetic field $\vec{H}_{||}$ of 0.2 T.

the growth. Owing to the thickness of the branches, the *in situ* observations at different scales, using the microscope, could not be conclusive and did not reveal the underlying fine features, if any, of the morphology of the deposits.

Arborescences of Co grown under $\vec{H}_{||}$ were examined by TEM combined with selected area ED [33]. As with Fe, except for some stacking faults in the crystal structure detected by ED, no specific features were observed that would reveal that $\vec{H}_{||}$ was applied during the growth.

VI. DISCUSSION

A number of processes are at work in the quasi-2D ECD of metals that are generally grouped in two main sets: that of kinetic transfer, including the chemical mechanisms as well as the surface phenomena at the growing front, and that of mass transport, by diffusion and migration, or through the electrolyte fluid motions (electroconvection, gravitoconvection, etc.). All these, qualitatively overviewed in Ref. [37], are still under active studies.

The influence of magnetic fields on the ECD processes have also been and continue to be considered by different investigators. Most of the experiments were not performed in the quasi-2D setup but should help to correctly interpret our observations.

A few works have concerned the kinetic transfer. Some field effects were earlier reported [38,39] but recent experiments [40,41] indicate that these are more of exceptions than the rule or perhaps arising from indirect mass transport, i.e., no significant field effects should in general be expected on kinetic transfer.

Much more works have concerned the mass transport. A magnetic field effect known for a long time [15] is the MHD convection, produced within the electrolyte, by the Lorentz body force $\vec{F}_{LB}=\vec{\mathcal{J}}\times\vec{B}$, locally orthogonal to the current density $\vec{\mathcal{J}}$ and to the induction $\vec{B}$ [31]. $\vec{F}_{LB}$ originates from the additive contributions of the Lorentz forces on the anions and cations and the efficient momentum transfers of these ions to the surrounding solvent. This convection in quasi-2D setup should arise only under normal magnetic field. Using engine oil emulsified within the electrolyte, we concretely checked this in our experiments. A different magnetic field induced convection involving charges was recently suggested [42]. Named electrokinetic (EK) MHD effect and confined on the nanometer scale region of the diffuse layer before the growth front, it would emerge from the EK field $\vec{E}_{EK}$ generated on applying the magnetic field normal to a current, as in Hall effect. $\vec{E}_{EK}$ is normal to both the magnetic field and the current. It is tangential to the diffuse layer where, owing to the excess charges, it gives rise to an EK body force $\vec{F}_{EK}$ producing the convection. This should occur under normal magnetic field and under in-plane magnetic field perpendicular to the local directions of growth.

Other existing body forces are those emerging from the gradient of the magnetic Zeeman energy. At room temperature this energy, for a unit volume of the electrolyte in the induction $\vec{B}$, is approximated as $\mathcal{N}(-\Sigma\chi_j C_j)(\vec{B}\cdot\vec{B})$, where the summation is extended over all the different species j of individual linear susceptibility χ_j and concentration C_j in the solution and $\mathcal{N}$ is the Avogadro number [43]. A magnetic Zeeman force that always exists then, owing to the concentration gradients, is $\vec{F}_{\vec{\nabla}C}=\mathcal{N}(\vec{B})^2(-\Sigma\chi_j\vec{\nabla}C_j)$. $\vec{F}_{\vec{\nabla}C}$ attract paramagnetic species towards and repel diamagnetic species from the regions of larger concentration. This force is large only within the diffusion layer where the concentration gradients exist. It is also clear that if an effect is induced by $\vec{F}_{\vec{\nabla}C}$, then this must not depend on the direction of $\vec{B}$. We have no indication of this in our experiments. It has been argued, by comparison to the driving force by diffusion in the diffusion layer, that $\vec{F}_{\vec{\nabla}C}$ would actually be of negligible influence [44]. The other magnetic Zeeman force that arises when the magnetic induction is not uniform [21] or when electrodes are magnetized [22,23] is $\vec{F}_{\vec{\nabla}\vec{B}}=2\mathcal{N}(-\Sigma\chi_j C_j)\times(\vec{B}\cdot\vec{\nabla}\vec{B})$. $\vec{F}_{\vec{\nabla}\vec{B}}$ attract paramagnetic species towards and repel diamagnetic species from the regions of larger induction. The field gradient of the magnetic mangle in our experiments gives rise to such a force but the growths in the electromagnet showed that this is not at all relevant. A more efficient contribution to $\vec{F}_{\vec{\nabla}\vec{B}}$ is that associated with the ferromagnetic nature of Fe and Co. Quite difficult to estimate, it could strongly influence the growths if the force is extended beyond the diffusion layer, i.e., if the growing branches are thick enough.

A. Normal fields

An outcome of the MHD convection in quasi-2D setup is that it almost always leads to a spiraling morphology and/or branch asymmetry of the deposits. As a surprise this is not the case at the macroscopic level in all of our Fe and Co growths under $\vec{H}_{\perp}$. Of course the deposits of similar growths of Zn, in the present work and previous ones [17] or of Cu [19] using exactly the same solvent and anion, show, under weak $\vec{H}_{\perp}$ amplitude, clearly always the spiraling and often the asymmetry. An explanation that first comes to mind would be that the Fe and Co growths are kinetic transfer controlled, but this would be contradictory with the growths of dendrites [45]. Other causes of inhibition could be the material hardness, but this for Cu and Zn is similar to that for Fe and Co, or the morphology, but both dense and sparse arborescences show neither the spiraling nor the asymmetry, except when the deposits consist of only two or three main branches.

Our growths show in fact different features at different scales. At the level of the TEM observations, we always observe single crystalline dendrites (Fig. 4) [33]. This indicates that the growths are both kinetic transfer and mass transport controlled. Under normal magnetic field, the Fe dendrites are bent while the Co crystal anisotropy is changed. The MHD convection would explain the first effect but not the second.

A specific feature of Fe and Co is in fact that they get magnetized under $\vec{H}_{\perp}$, but for the considered fields are magnetically not fully saturated along it [25]. We thus get a complex distribution of magnetic moments with both normal and in-plane components leading to as complex magnetic dipolar

interactions inside the deposit. A detailed analysis of these interactions would be challenging for involving the unsaturated magnetization distribution of a growing deposit, the morphology of which is not only very irregular but also evolving in time. Some growth rigidity should be expected, increasing with the size of the deposit as expected from dipolar interactions and inhibiting the spiraling above some scale. Another possibility, also complex to evaluate, would be that the $\vec{F}_{\vec{\nabla}\vec{B}}$ force arising from the growing deposit magnetization is sufficiently extended to thwart the MHD convection beyond the diffusion layer.

At the scale of the observations with the microscope, all the growths under $\vec{H}_{\perp}$ show a common feature, besides the mechanical branch breakings due to the fluid stirring: there is an increase in the branch separations of the deposits. On the analogy of interbranch electroconvection in the growths from acidified solutions [27], specific $\vec{H}_{\perp}$-induced local fluid motions at the growing fronts, which would favor the branch separations, cannot *a priori* be fully ruled out. Nevertheless, the growths from solutions with emulsified engine oil did not detect any additional fluid motion that would not be ascribable to the MHD convection. A more plausible cause of the increase in the branch separations appear to be the magnetic dipolar interactions between the branches, which under $\vec{H}_{\perp}$ get magnetized. Assimilating the branches to thin cylinders, the morphology features observed under $\vec{H}_{\perp}$ can be qualitatively understood: nearby branches magnetized in the same direction will tend to repel each other while magnetized in opposite directions will tend to attract each other. Magnetization measurements were performed that confirmed that the Fe and Co arborescences are both ferromagnetic at 20 °C but that the magnetization saturates for $\vec{H}_{\perp}$ amplitudes larger than 0.2 T [25]. Around this value, the magnetization of the thinner and/or longer branches still lie close to either of the directions, in the plane of the growth, along which they are elongated, rather than along $\vec{H}_{\perp}$. Accordingly a probability exists that nearby such branches are dominantly magnetized in opposite directions. As observed in the sparse arborescences, this would explain that thin branches tend to collapse over each other to form thick branches while these tend rather to separate from each other. The collapse should disappear at large $\vec{H}_{\perp}$. It is not observed in the dense arborescence, which is consistent with the fact that magnetic saturation in these arborescences is achieved at lower $\vec{H}_{\perp}$ [25] but also partly because the thinnest branches are probably close to collapse over each other. Of course the magnetization of a branch under an unfavorable magnetic dipolar environment could as well simply reverse itself. We have not taken into account such local flips of moments but this is basically not going to change the above reasoning except by making it more complex.

B. In-plane fields

Completely different features are observed when the in-plane magnetic field $\vec{H}_{||}$ is applied. Almost no influence is found out at the level of the TEM observations except for an increased tendency to the formation of more needlelike branches for Fe and crystal defects for Co. What would be the cause of that is unclear. With the induction at contact of a branch locally dominated by the field contribution from the branch magnetization, the EK MHD convection should not be relevant. An influence of $\vec{F}_{\vec{\nabla}\vec{B}}$, which would slightly modify the diffusion layer, is thus not excluded, at least for favoring more needlelike branches in connection with its directional feature. A local MHD convection could also exist if a gravitoconvection were to occur, but this was not detected. Clearly, the field effects at this scale are of no help to interpret those effects at the macroscopic level, i.e. the circle to rectangle morphology symmetry breaking for the dense arborescences and the isotropic to stringy pattern symmetry reduction for the sparse arborescences.

Qualitatively, the easiest instance to understand is that of the $\vec{H}_{||}$-induced formation of stringy pattern parallel to the field. It is clear that the orientation of the deposit minimizes the magnetostatic interactions similarly as a compass needle would along a magnetic field. Magnetization measurements on growths without magnetic field showed that saturation is still not achieved for an $\vec{H}_{||}$ amplitude of 0.2 T [25,46], implying that the moments are not fully aligned along the field and some branches have their magnetization, and therefore the induction at the growth front, more along their direction of growths than along $\vec{H}_{||}$. The outcome of this is that $\vec{F}_{\vec{\nabla}\vec{B}}$ can hardly be the cause of the stringy pattern. As already stated it appears actually that to minimize the Zeeman energy of the magnetized deposit under $\vec{H}_{||}$, all the branches growing at a direction different from the field mechanically twist to get parallel to $\vec{H}_{||}$ and bind with the others.

The ''circle to rectangle'' morphology symmetry breaking could be interpreted, from the observations using the microscope, as arising from growths of branches at a definite angle from a fixed direction from $\vec{H}_{||}$ or its perpendicular. With branches growing at the same speed this leads to pairs of parallel straight fronts perpendicular and parallel to $\vec{H}_{||}$, giving rise to a deposit of rectangular global shape if the growths along and perpendicular to $\vec{H}_{||}$ differ. Such an asymmetry is found out up to the highest $\vec{H}_{||}$ amplitude as produced by the electromagnet (1.6 T). The formation of pairs of parallel straight fronts is expected to be a rather trivial pattern feature of dendritic growths in low noise environments, as in dendritic ice crystal grown in undercooled pure water [11]. A 2θ angle of 60° and three fixed directions at 60° from each other are involved in this ice growth, giving rise to an arborescence entirely single crystalline with a hexagonal external envelope. An angle of 60° is consistent with the fcc structure of Fe, provided that the $\langle 111 \rangle$ direction is perpendicular to the plane of growth. What is rather unusual in the growths of the dense Fe arborescences under $\vec{H}_{||}$ is that only two pairs of parallel growth fronts are involved that are perpendicular to each other while formed from same angles as that in ice and anyway not complementary to each other, i.e., $2\phi + 2\psi \neq 180°$. Accordingly the deposit is necessarily not a single crystal and consists most probably in a textured polycrystal reflecting the symmetry of two single crystals

oriented perpendicular to each other. A well defined branching angle is actually also observed in growths without magnetic field but the orientation of the branches is only local and not preserved over large distances. According to the previous investigations without magnetic field of quasi-2D ECD of Fe from $Fe(SO_4)$ aqueous solutions, an oscillatory accumulation and depletion of H_3O^+ ions in front of the growing interface could occur, which would cause alternating transitions between dendritic and tip-splitting growths [26]. Subsequent experiments with acidified electrolytes [27,47] demonstrated that these ions can indeed be strongly influential on the growth through changes in the interfacial free energy and/or initiation of interbranch electroconvection. Although the growth conditions attached to these experiments are different from ours (parallel geometry vs circular geometry, constant current vs constant voltage, etc.), an intermittent change in time of the concentration of H_3O^+ ions at the growing front of our deposits cannot be ruled out, and the chaotic blocking/initialization of a dendritic growth by a local increase/decrease of this concentration is not unlikely. This could be a plausible noise leading to the loss of correlations at large scale in the branch orientation of the dense arborescences. Additionally, the growth, occurring in a fluid medium, can be perturbed by convections of different origins. Under $\vec{H}_{||}$ these noises could be reduced for some reason allowing for large scale crystal coherence, but this should rather lead to a single crystal with a hexagonal external envelope, such as for dendritic ice, since the branching angle is 60°. To explain why the $\vec{H}_{||}$ direction and the direction perpendicular to it in the plane of the growth are especially selected, magnetostatic interactions between the branches and of the branches with $\vec{H}_{||}$ should necessarily be taken into account. A detailed analysis would again be too complex, but numerical estimates of energy can be made for different morphologies at constant mass by assimilating the branches with thin cylinders or lines of magnetic dipoles. It is then found out that the overall magnetic energy can be minimized for needles at 60°, growing symmetrically with respect, not only, as intuitively expected, to the perpendicular direction to $\vec{H}_{||}$, but also with respect to the $\vec{H}_{||}$ direction. A dendrite that would grow with its central nerve along $\vec{H}_{||}$ and secondary branches at 60° of this direction is then not favored, in agreement with the experiment. Could the morphology observed under $\vec{H}_{||}$ emerge solely from the minimization of the magnetic dipolar energy between the branches and of the Zeeman energy of the branches with $\vec{H}_{||}$, under the constraints of the crystalline anisotropy, or should a simultaneous noise reduction be necessary as well, is not clear.

VII. CONCLUSION

Systematic quasi-2D ECD of Fe and Co arborescences were performed under normal $\vec{H}_{\perp}$ and in-plane $\vec{H}_{||}$ magnetic fields mostly up to 0.2 T. On the same growth, the morphology and structure of the deposits as examined by TEM fully differed from those observed macroscopically or using a microscope. A scale above which additional effects of the field come out is thus evidenced. Our analysis of the different instances showed that these additional effects arise from the magnetic dipolar interactions inside the magnetized deposit and of the magnetic Zeeman interactions of this with the applied field. Applied to isolated spins or disordered ones these interactions would be weak, but owing to the ferromagnetism of the deposits they become dominant over a certain scale.

[1] *Branching in Nature*, edited by V. Fleury, J.-F. Gouyet, and M. Leonetti (Springer-Verlag, Berlin and EDP Sciences, Les Ulis, 2001).

[2] M.C. Cross and P.C. Hohenberg, Rev. Mod. Phys. **65**, 851 (1993).

[3] T. Viscsek, *Fractal Growth Phenomena* (World Scientific, Singapore, 1989).

[4] R.C. Brady and R.M. Ball, Nature (London) **309**, 225 (1984).

[5] M. Matsushita, M. Sano, Y. Hayakawa, H. Honjo, and Y. Sawada, Phys. Rev. Lett. **53**, 286 (1984).

[6] Y. Sawada, A. Dougherty, and J.P. Gollub, Phys. Rev. Lett. **56**, 1260 (1986).

[7] D. Grier, E. Ben-Jacob, R. Clarke, and L.M. Sander, Phys. Rev. Lett. **56**, 1264 (1986).

[8] M. Matsushita, Y. Hayakawa, and Y. Sawada, Phys. Rev. A **32**, 3814 (1985).

[9] F. Argoul, A. Arneodo, G. Grasseau, and H.L. Swinney, Phys. Rev. Lett. **61**, 2558 (1988).

[10] T.A. Witten and L.M. Sander, Phys. Rev. Lett. **47**, 1400 (1981); Phys. Rev. B **27**, 5686 (1983).

[11] J.S. Langer, Rev. Mod. Phys. **52**, 1 (1980).

[12] D.G. Grier, D.A. Kessler, and L.M. Sander, Phys. Rev. Lett. **59**, 2315 (1987).

[13] D. Barkey, J. Electrochem. Soc. **138**, 2912 (1991).

[14] J.O'M. Bockris and A.K.N. Reddy, *Modern Electrochemistry* (Plenum, New York, 1973).

[15] T.Z. Fahidy, J. Appl. Electrochem. **13**, 553 (1983), and references cited therein.

[16] R.A. Tacken and L.J.J. Janssen, J. Appl. Electrochem. **25**, 1 (1995), and references cited therein.

[17] I. Mogi, M. Kmamiko, S. Okubo, and G. Kido, Physica B **201**, 606 (1994).

[18] I. Mogi and M. Kmamiko, J. Phys. Soc. Jpn. **64**, 4500 (1995).

[19] J.M.D. Coey, G. Hinds, and M.E.G. Lyons, Europhys. Lett. **47**, 267 (1999).

[20] M. Waskaas and Y.I. Kharkats, J. Phys. Chem. B **103**, 4876 (1999).

[21] S.R. Ragsdale, K.M. Grant, and H.S. White, J. Am. Chem. Soc. **120**, 13461 (1998).

[22] M.D. Pullins, K.M. Grant, and H.S. White, J. Phys. Chem. B **105**, 8989 (2001).

[23] N. Leventis and X. Gao, J. Am. Chem. Soc. **124**, 1079 (2002).

[24] S. Bodea, L. Vignon, R. Ballou, and P. Molho, Phys. Rev. Lett. **83**, 2612 (1999).

[25] S. Bodea, Ph.D. thesis, Université Joseph Fourier, Grenoble, France, 2000.
[26] M. Wang and N.B. Ming, Phys. Rev. Lett. **71**, 113 (1993).
[27] M. Wang, W.J.P. van Enckevort, N. Ming, and P. Bennema, Nature (London) **367**, 438 (1994).
[28] V. Fleury, M. Rosso, J.-N. Chazalviel, and B. Sapoval, Phys. Rev. A **44**, 6693 (1991).
[29] Provided by Sigma-Aldrich (www.sigma-aldrich.com).
[30] O. Cugat, P. Hansson, and J.M.D. Coey, IEEE Trans. Magn. **30**, 4602 (1994).
[31] All the magnetic fields $\vec{H}$ and magnetizations $\vec{M}$ are implicitly multiplied by the permeability $\mu_0 = 4\pi \times 10^{-7}$ T/(A/m) of the free space and given in tesla. The magnetic flux density or magnetic induction $\vec{B}$ in any medium is then obtained as $\vec{B} = \vec{H} + \vec{M}$. Within a diamagnetic or a paramagnetic substance, this is simplified to $\vec{B} \approx (1+\chi)\vec{H} \approx \vec{H}$, where χ is the linear magnetic susceptibility of the substance.
[32] Y. Sawada and H. Hyosu, Physica D **38**, 299 (1989).
[33] S. Bodea, R. Ballou, L. Pontonnier, and P. Molho, Phys. Rev. B **66**, 224104 (2002).
[34] See http://www.merck.de/english/services/chemdat/english/index.htm
[35] J.M. Huth, H.L. Swinney, W.D. McCormick, A. Kuhn, and F. Argoul, Phys. Rev. E **51**, 3444 (1995).
[36] G. Helgesen, A.T. Skjeltorp, P.M. Mors, R. Botet, and R. Julien, Phys. Rev. Lett. **61**, 1736 (1988).
[37] F. Argoul and A. Kuhn, Physica A **213**, 209 (1995).
[38] C. Iwakura, M. Kitayama, T. Edamoto, and H. Tamura, Electrochim. Acta **30**, 747 (1985).
[39] R. Aogaki, T. Negishi, M. Yamato, E. Ito, and I. Mogi, Physica B **201**, 611 (1994).
[40] G. Hinds, J.M.D. Coey, and M.E.G. Lyons, J. Appl. Phys. **83**, 6447 (1998).
[41] O. Devos, O. Aaboubi, J.P. Chopart, and A. Olivier, Nonlinear J. Phys. Chem. A **104**, 1544 (2000).
[42] A. Olivier, J.P. Chopart, J. Amblard, E. Merrienne, and O. Aaboubi, ACH-Models Chem. **137**, 213 (2000).
[43] N. Leventis and X. Gao, Anal. Chem. **73**, 3981 (2001).
[44] C. O'Reilly, G. Hinds, and J.M.D. Coey, J. Electrochem. Soc. **148**, 674 (2001); G. Hinds, F.E. Spada, J.M.D. Coey, T.R. NíMhíochàin, and M.E.G. Lyons, J. Phys. Chem. **105**, 9487 (2001).
[45] R.F. Voss and M. Tomkiewicz, J. Electrochem. Soc. **132**, 371 (1985).
[46] S. Bodea, V. Heresanu, R. Ballou, and P. Molho, J. Magn. Magn. Mater. **226-230**, 1978 (2001).
[47] K.Q. Zhang, M. Wang, S. Zhong, G.X. Chen, and N.B. Ming, Phys. Rev. E **61**, 5512 (2000); K. Zhang, M. Wang, R. Peng, Y. Xiao, and N. Ming, Phys. Lett. A **278**, 286 (2001).